

## Article

# Synthesis, Crystal Structure and Supramolecular Features of Novel 2,4-Diaminopyrimidine Salts

Joanna Bojarska <sup>1</sup>, Krzysztof Łyczko <sup>2</sup> and Adam Mieczkowski <sup>3,\*</sup>

<sup>1</sup> Institute of General and Ecological Chemistry, Faculty of Chemistry, Lodz University of Technology, Zeromskiego 116, 90-924 Lodz, Poland; joanna.bojarska@p.lodz.pl

<sup>2</sup> Institute of Nuclear Chemistry and Technology, Dorodna 16, 03-195 Warsaw, Poland; k.lyczko@ichtj.waw.pl

<sup>3</sup> Institute of Biochemistry and Biophysics, Polish Academy of Sciences, Pawinskiego 5a, 02-106 Warsaw, Poland

\* Correspondence: amiecz@ibb.waw.pl

**Abstract:** The crystal structures and the supramolecular architectures of a series of novel salts originating from 2,4-diaminopyrimidine and four different chain dicarboxylic acids are reported. For this purpose, 2,4-diaminopyrimidin-1-ium 2,2'-thio(acetic)acetate (**1**), 2,4-diaminopyrimidin-1-ium monoglutarate (**2**), 2,4-diaminopyrimidin-1-ium 3,3'-dithio(propionic)propionate (**3**) and 2,4-diaminopyrimidin-1-ium suberate (**4**) were synthesized in good to high yields from 2,4-diaminopyrimidine and appropriate dicarboxylic acids (2,2'-thiodiacetic acid, glutaric acid, 3,3'-dithiodipropionic acid and suberic acid, respectively). Each of the compounds were formed as a monohydrate and compound **4** additionally co-crystallized with the suberic acid molecule. Despite the similar structures of compounds **1** and **2** as well as **3** and **4**, subtle but important differences are observed in their crystal packing and H-bonding patterns, especially between **3** and **4**. Supramolecular self-assemblies can be distinguished through different interactions considering anions, leading to diverse H-bonding motifs, which also include sulphur atoms in **1** and **3**, at the upper level of supramolecular architecture. Notably, the basic motif is always the same—2,4-diaminopyrimidine-based homosynthon  $R^2_2(8)$  via N-H...N interactions. The impact of diverse types of intermolecular interactions was evaluated by Hirshfeld analysis, while the propensity of atom pairs of elements to build interactions was calculated using enrichment ratios. Although compounds **1** and **3** contain S-atoms, the percentage of S-derived interactions is rather low. In **1**, the contribution of S...H/H...S, S...C/C...S, S...N/N...S intermolecular contacts is 5.7%. In **2**, the contribution of S...H/H...S accounts for only 0.6%.

**Keywords:** pyrimidine; synthesis; crystal structure; supramolecular synthon; Hirshfeld surface; electrostatic potential; enrichment ratio



**Citation:** Bojarska, J.; Łyczko, K.; Mieczkowski, A. Synthesis, Crystal Structure and Supramolecular Features of Novel 2,4-Diaminopyrimidine Salts. *Crystals* **2024**, *14*, 133. <https://doi.org/10.3390/cryst14020133>

Academic Editors: Etsuo Yonemochi and Tom Leyssens

Received: 28 December 2023

Revised: 19 January 2024

Accepted: 25 January 2024

Published: 28 January 2024



**Copyright:** © 2024 by the authors. Licensee MDPI, Basel, Switzerland. This article is an open access article distributed under the terms and conditions of the Creative Commons Attribution (CC BY) license (<https://creativecommons.org/licenses/by/4.0/>).

## 1. Introduction

The 2,4-diaminopyrimidine group is present in many bioactive molecules and drugs. One of the simplest analogues—2,4-diaminopyrimidine 3-oxide (2,4-DPO, Kopexil) and its derivative, Minoxidil are used in hair loss treatment to reduce hair shedding and increase hair mass and density [1]. The other examples of bioactive substances possessing the 2,4-diaminopyrimidine group include but are not limited to dihydrofolate reductase inhibitor drugs used to treat parasitic diseases (pyrimethamine, trimetrexate) [2], bacterial infections (iclaprim, trimethoprim) [2] or they as anticancer agents [3]. In the latter case, inhibitors of focal adhesion kinase [4,5] could be a good example.

Due to the importance of pyrimidine compounds in organic and medicinal chemistry, we have conducted research to extend our knowledge of the supramolecular features of 2,4-diaminopyrimidine compounds. Until now, the 2,4-diaminopyrimidin-1-ium cation has been presented in salts with simple inorganic ( $\text{Cl}^-$ ,  $\text{ClO}_4^-$ ,  $\text{NO}_3^-$ ,  $\text{SeO}_4^{2-}$  and  $\text{HPO}_4^{2-}$  [6]) and some organic anions (1,3-cyclopentanedionate, 1,3-cyclohexanedionate [7], 4-nitrophenolate [8], barbiturate, 2-thiobarbiturate [9], two 2-thiouracilate derivatives [10] and 2,8-dioxo-2,7,8,9-tetrahydro-1H-purin-6-olate [11]).

In recent years, much attention has been paid to crystals containing the 2,4-diaminopyrimidin-1-ium-carboxylate supramolecular heterosynthon [12]. Its energy is quite high (>50 kJ/mol [13]) and it plays a structure-directing role in various single- and multicomponent crystals [14–17].

In cocrystal hydrates, the role of the water molecule in the supramolecular organization was discovered [18]. The total enthalpy of H-bonds formed by a water molecule is about 90 kJ/mol [19]. The structure-directing role of water was further identified in pharmaceutical multicomponent crystals [20] and organic multicomponent crystals [21].

Here, we report the synthesis and crystallographic investigations of four new salts, namely, 4-diaminopyrimidin-1-ium 2,2'-thio(acetic)acetate (1), 2,4-diaminopyrimidin-1-ium monoglutarate (2), 2,4-diaminopyrimidin-1-ium 3,3'-dithio(propionic)propionate (3), 2,4-diaminopyrimidin-1-ium suberate suberic acid (4), see Figure 1. The crystal packing and topology of H-bonding networks are investigated by Hirshfeld surface analysis, which is a leading method to detect all possible intermolecular interactions that control the crystal structure.

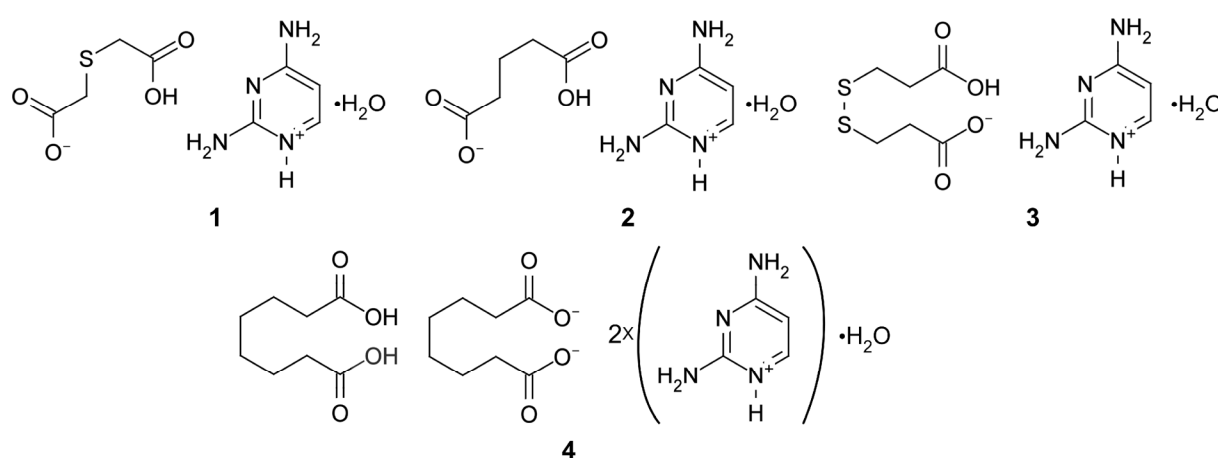


**Figure 1.** Structures of analysed salts: 2,4-diaminopyrimidin-1-ium 2,2'-thio(acetic)acetate monohydrate (1), 2,4-diaminopyrimidin-1-ium monoglutarate monohydrate (2), 2,4-diaminopyrimidin-1-ium 3,3'-dithio(propionic)propionate monohydrate (3), 2,4-diaminopyrimidin-1-ium suberate suberic acid monohydrate (4).

## 2. Materials and Methods

### 2.1. Synthesis of Compounds 1–4

The commercially available chemicals were of reagent grade and used as received. The following procedures were applied to obtain requested crystals of 2,4-diaminopyrimidine salts.

*2,4-diaminopyrimidin-1-ium 2,2'-thio(acetic)acetate monohydrate (1)*: 11 mg of 2,4-diaminopyrimidine (0.1 mmol, 1 equiv.) and 15 mg (0.1 mmol, 1 equiv.) of 2,2'-thiodiacetic acid were dissolved in 2 mL of warm distilled water, the solution was filtered through a small cotton pad and left in the room temperature for solvent evaporation (about two weeks). The obtained crystals of salts were used in the X-ray measurements.

*2,4-diaminopyrimidin-1-ium monoglutarate monohydrate (2)*: 11 mg of 2,4-diaminopyrimidine (0.1 mmol, 1 equiv.) and 13 mg (0.1 mmol, 1 equiv.) of glutaric acid were dissolved in 2 mL of warm distilled water, the solution was filtered through a small cotton pad and left in the room temperature for solvent evaporation (about two weeks). The obtained crystals of salts were used in the X-ray measurements.

*2,4-diaminopyrimidin-1-ium 3,3'-dithio(propionic)propionate monohydrate (3)*: 11 mg of 2,4-diaminopyrimidine (0.1 mmol, 1 equiv.) and 21 mg (0.1 mmol, 1 equiv.) of 3,3'-dithiodipropionic acid were dissolved in 2 mL of warm distilled water, the solution was filtered through a small cotton pad and left in the room temperature for solvent evaporation (about two weeks). The obtained crystals of salts were used in the X-ray measurements.

*2,4-diaminopyrimidin-1-ium suberate suberic acid monohydrate (4)*: 11 mg of 2,4-diaminopyrimidine (0.1 mmol, 1 equiv.) and 13 mg (0.1 mmol, 1 equiv.) of suberic acid were dissolved in

2 mL of warm distilled water, the solution was filtered through a small cotton pad and left in the room temperature for solvent evaporation (about two weeks). The obtained crystals of salts were used in the X-ray measurements.

## 2.2. Single-Crystal X-ray Diffraction

Good quality single-crystals of **1–4** were selected for the X-ray diffraction experiments at  $T = 100$  K. X-ray diffraction data were collected on a Rigaku SuperNova (dual source) four-circle diffractometer equipped with an Eos CCD detector using a mirror-monochromated Cu  $K\alpha$  radiation ( $\lambda = 1.54184$  Å) from a microfocus Nova X-ray source. CrysAlis PRO software (version 1.171.40.84a) was used to perform all operations, including data collection and reduction, and multi-scan absorption correction. The structures were solved by direct methods and refined by full matrix least-squares treatment on  $F^2$  data. Hydrogen atoms bonded to carbon atoms were placed in calculated positions and refined isotropically as a riding model with standard parameters. The H atoms bonded to the N and O atoms were located from a difference Fourier map, and their positions were freely refined. All other atoms were refined with anisotropic atomic displacement parameters. All calculation procedures were performed using SHELXTL programs [22], cooperating with the OLEX2 crystallographic software (version 1.5) [23]. Mercury [24] program was applied for the graphical representation of the structures.

## 2.3. Computational Details

Geometry analysis and molecular diagrams were generated using the Mercury [24] and PLATON [25] programs. The 3D Hirshfeld surfaces and 2D fingerprints calculations were performed in CrystalExplorer 17.5 [26], based on the methods reported in the literature [27], using CIF's archives collected of **1–4** crystal structures. The graphs of Hirshfeld's surfaces were mainly mapped with  $d_{norm}$  property using a scheme of colours: red dots illustrate the shortest contacts, the white areas indicate intermolecular distances close to the van der Waals (vdW) contacts (with  $d_{norm}$  equal to zero), while the blue regions show the contacts longer than the sum of the vdW radii (with positive values of  $d_{norm}$ ) [22,27]. The  $d_{norm}$ -map was generated by calculating the normalised distances from the contact points on the Hirshfeld surface to the nearest nucleus inside (denoted as  $d_i$ ) or outside ( $d_e$ ) the surface upon the adaption of all H-bond length to the neutron-derived values [28]. Fingerprint plots present a qualitative description of all contacts in the crystal, as a function of  $d_i$  and  $d_e$  values [27]. The enrichment ratios (ER) of the interactions available in the analysed crystal structures were calculated on the basis of the HS methodology [29]. Both privileged and disfavoured intermolecular contacts were highlighted in the crystal structures.

## 3. Results and Discussion

### 3.1. Structural Commentary

Crystals of **1–4** were obtained, and their structures were established by X-ray crystallography. The X-ray molecular structures are presented in Figures 2–5.

The compounds **1** and **4** crystallize in the triclinic space group  $P\bar{1}$ , while compounds **2** and **3** crystallize in the monoclinic centrosymmetric space groups  $P2_1/c$  and  $C2/c$ , respectively. The asymmetric units in **1–3** consist of one 2,4-diaminopyrimidin-1-ium cation and one dicarboxylic acid molecule in the form of monoanion (2,2'-thio(acetic)acetate, monoglutarate and 3,3'-dithio(propionic)propionate, respectively) as well as one solvent (water) molecule. In **1**, one hydrogen atom of the water molecule is located over two possible positions. Unlike **1–3**, the asymmetric unit in **4** contains, in addition to the 2,4-diaminopyridin-1-ium cation, half of the suberate anion and half of the suberic acid molecule which both are located on an inversion centre. The crystallographic data of studied salts are summarized in Table 1.

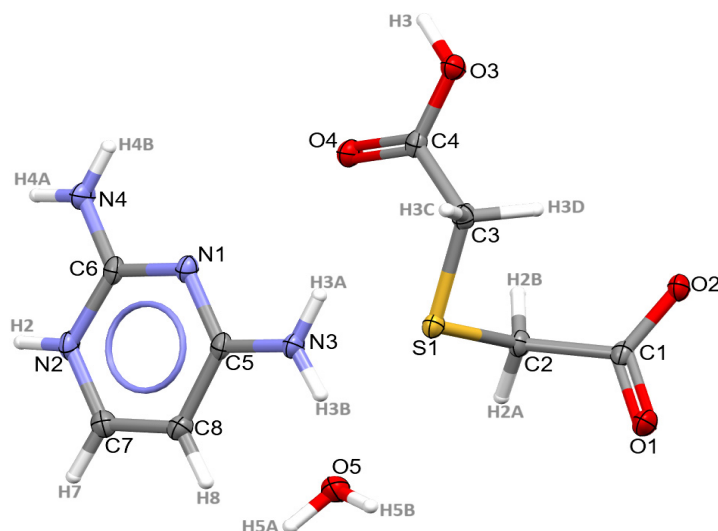


Figure 2. Molecular structure of 1 at a 30% probability level showing the atom numbering scheme.

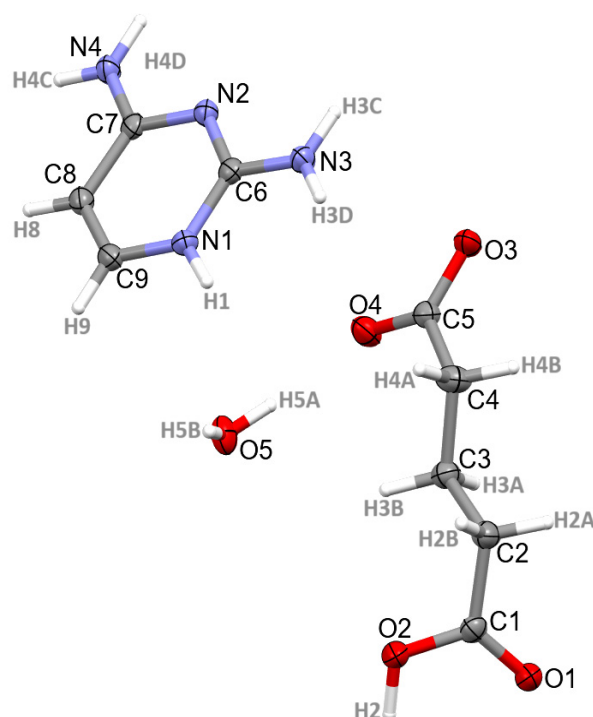


Figure 3. Molecular structure of 2 at a 30% probability level showing the atom numbering scheme.

Table 1. Crystallographic data and structure refinement parameters for the studied compounds.

Compound	1	2	3	4
Chemical formula	$C_8H_{14}N_4O_5S$	$C_9H_{16}N_4O_5$	$C_{20}H_{34}N_8O_9S_4$	$C_{24}H_{44}N_8O_{10}$
Formula weight	278.29	260.26	658.79	604.67
$\lambda$ (Cu $K\alpha$ ) (Å)	1.54184	1.54184	1.54184	1.54184
Crystal system	triclinic	monoclinic	monoclinic	Triclinic
Space group	$P\bar{1}$	$P2_1/c$	$C2/c$	$P\bar{1}$
$a$ (Å)	4.78960(16)	4.85263(11)	31.6649(8)	5.3664(4)
$b$ (Å)	10.5175(3)	26.0403(5)	5.10031(11)	9.2521(5)
$c$ (Å)	12.6651(4)	9.8003(2)	18.3024(4)	15.2231(9)
$\alpha$ (°)	107.397(3)	90	90	93.347(5)
$\beta$ (°)	95.472(3)	96.4945(19)	93.141(2)	94.615(6)

Table 1. Cont.

Compound	1	2	3	4
$\gamma$ (°)	102.363(3)	90	90	102.566(6)
Volume (Å <sup>3</sup> )	585.94(3)	1230.46(5)	2951.41(12)	733.10(9)
Z	2	4	4	1
Z'	1	1	0.5	0.5
$D_{\text{calc}}$ (g·cm <sup>-3</sup> )	1.577	1.405	1.483	1.370
$\mu$ (mm <sup>-1</sup> )	2.700	0.986	3.499	0.902
F (000)	292	552	1384	324
Crystal size (mm)	0.28 × 0.15 × 0.04	0.20 × 0.12 × 0.03	0.20 × 0.14 × 0.05	0.18 × 0.10 × 0.04
$\theta$ range (°)	3.712–70.035	3.394–70.311	2.795–69.226	2.921–70.572
Reflections collected	15217	13019	17911	5322
Unique reflections	2178	2308	2738	2740
Reflections $I > 2\sigma(I)$	1992	2064	2648	2192
$R_{\text{int}}$	0.0323	0.0253	0.0246	0.0247
Restraints/parameters	1/193	0/195	0/214	0/222
Goodness-of-fit	1.035	1.050	1.059	1.035
$R_1, wR_2$ ( $I > 2\sigma(I)$ )	0.0305, 0.0347	0.0344, 0.0391	0.0234, 0.0241	0.0488, 0.0630
$R_1, wR_2$ (all data)	0.0770, 0.0810	0.0885, 0.0932	0.0633, 0.0639	0.1260, 0.1373
Max. peak/hole (e·Å <sup>-3</sup> )	0.369/−0.346	0.260/−0.219	0.277/−0.200	0.661/−0.440
K.P.I. (%) *	74.7	69.9	70.4	71.3

\* K.P.I.—Kitajgorodski packing index.

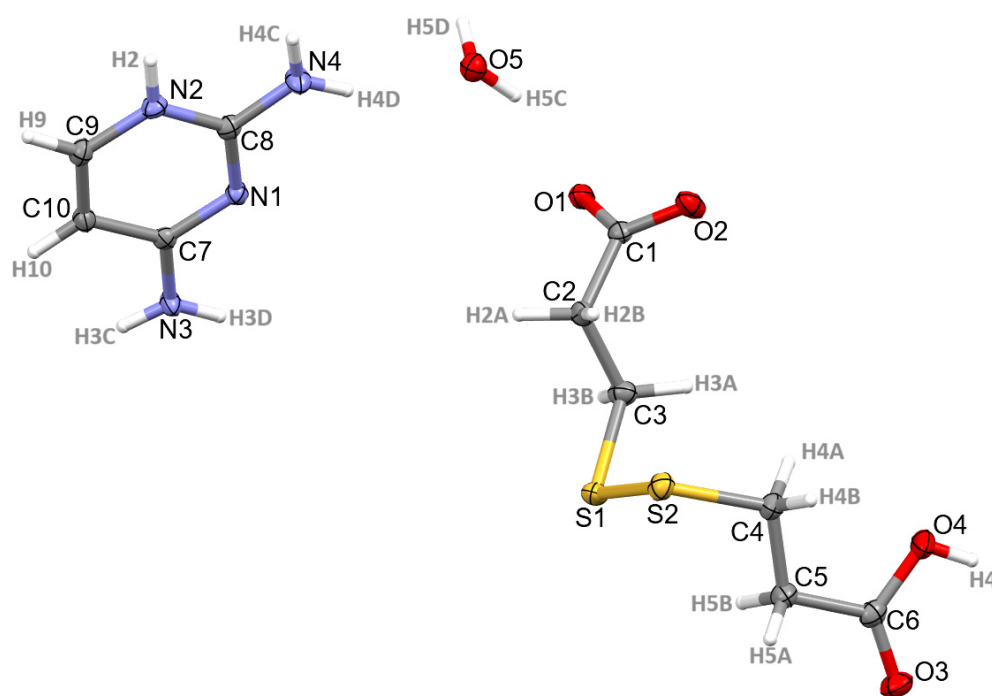


Figure 4. Molecular structure of 3 at a 30% probability level showing the atom numbering scheme.

All the investigated structures have a planar 2,4-diaminopyrimidin-1-ium moiety with the possibility of formation of diverse H-bonding—or  $\pi$ -stacking interactions. The crystal packing in all systems is driven by O-H $\cdots$ O, N-H $\cdots$ O, N-H $\cdots$ N, and C-H $\cdots$ O interactions and in 3 additionally by C-H $\cdots$ S contacts. The donor-to-acceptor distances vary from 1.97 Å for N-H $\cdots$ O in 3 to 3.52 Å for C-H $\cdots$ O in 4. The geometric parameters associated with intra- and intermolecular H-bonding of 1–4 are shown in Table 2, while  $\pi$ -based intermolecular interactions are listed in Tables S1 and S2 (Supplementary Materials).

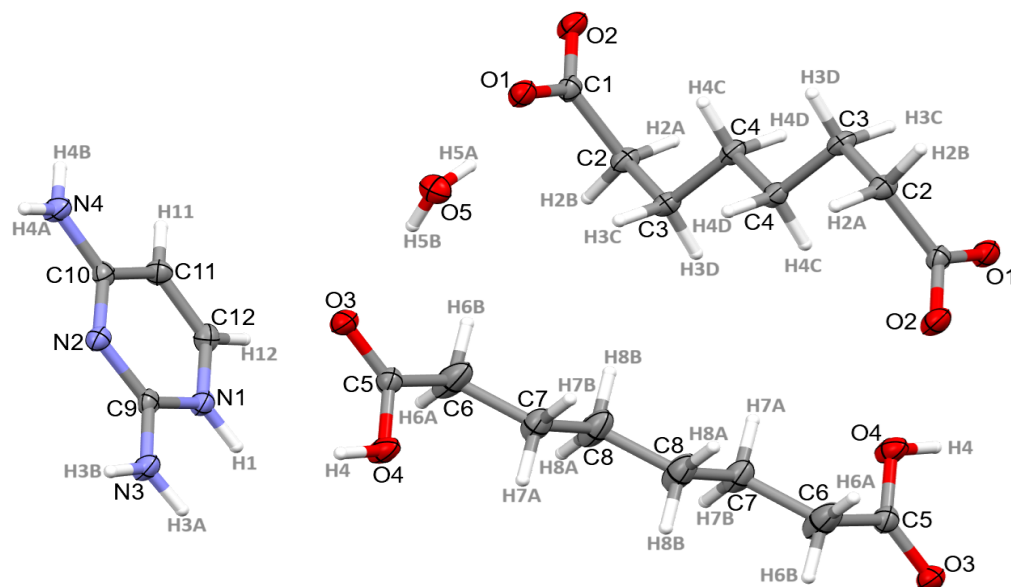


Figure 5. Molecular structure of 4 at a 30% probability level showing the atom numbering scheme.

Table 2. Geometric parameters of H-bonds for 1–4.

D-H...A	d(D-H)	d(H...A)	d(D...A)	<(DHA)	Symmetry Code
<b>1</b>					
N2-H2...O2	0.87(2)	1.87(2)	2.7375(18)	172.2(18)	$x, -1 + y, z$
O3-H3...O2	0.96(2)	1.57(2)	2.5218(15)	175.2(18)	$1 - x, 1 - y, -z$
N3-H3A...O4	0.87(2)	2.21(2)	3.0757(18)	170.2(19)	$-1 + x, y, z$
N3-H3B...O5	0.86(2)	2.11(2)	2.9540(18)	169.9(18)	$-1 + x, y, z$
N4-H4A...O4	0.85(2)	2.141(19)	2.8473(19)	140.0(16)	$1 - x, -y, -z$
N4-H4B...N1	0.85(2)	2.17(2)	3.018(2)	174.4(19)	$-x, -y, -z$
O5-H5A...O1	0.85	1.97	2.8111(18)	173	$1 - x, 1 - y, 1 - z$
O5-H5B...O5	0.85	2.16	2.991(2)	164	$2 - x, 1 - y, 1 - z$
O5-H5C...O5	0.85	2.18	3.012(2)	166	$1 - x, 1 - y, 1 - z$
C2-H2B...O3	0.99	2.41	3.1713(19)	133	$1 - x, 1 - y, -z$
C3-H3C...O4	0.99	2.31	3.2956(19)	175	$-1 + x, y, z$
<b>2</b>					
N1-H1...O3	0.93(2)	1.80(2)	2.7207(15)	171.6(17)	$-1 + x, y, z$
N1-H1...O4	0.93(2)	2.51(2)	3.1815(14)	129.0(15)	$-1 + x, y, z$
O2-H2...O3	0.97(2)	1.60(2)	2.5647(14)	171(2)	$-1 + x, \frac{1}{2} - y, -1/2 + z$
N3-H3C...N2	0.893(19)	2.078(18)	2.9679(17)	174.5(17)	$2 - x, 1 - y, 1 - z$
N3-H3D...O1	0.877(18)	2.103(17)	2.8148(16)	137.8(16)	$x, \frac{1}{2} - y, \frac{1}{2} + z$
N4-H4C...O5	0.898(18)	1.925(18)	2.8214(15)	175.3(18)	$1 - x, 1 - y, -z$
N4-H4D...O1	0.909(19)	2.060(19)	2.9605(14)	170.7(16)	$2 - x, \frac{1}{2} + y, \frac{1}{2} - z$
O5-H5A...O4	0.87(3)	1.96(3)	2.8160(14)	171(2)	
O5-H5B...O4	0.86(2)	2.04(2)	2.8973(14)	172(2)	$-1 + x, y, z$
C4-H4B...O2	0.99	2.51	3.2596(17)	132	$1 + x, \frac{1}{2} - y, \frac{1}{2} + z$
<b>3</b>					
N2-H2...O2	0.84	1.92	2.7553(13)	172	$1 - x, 1 + y, \frac{1}{2} - z$
N3-H3C...O1	0.85	2.14	1.9730(12)	168	$1 - x, 1 - y, 1 - z$
N3-H3D...N1	0.87	2.17	3.0322(14)	175	$1 - x, 1 - y, 1 - z$
O4-H4...O2	0.83	1.78	2.6053(14)	174	$3/2 - x, -1/2 + y, \frac{1}{2} - z$
N4-H4C...O1	0.84	2.08	2.9087(12)	170	$1 - x, 1 + y, \frac{1}{2} - z$
O5-H5C...O1	0.87	1.87	2.7334(10)	174	$1 - x, y, \frac{1}{2} - z$
O5-H5D...O1	0.87	1.93	2.7334(10)	153	
*C5-H5B...S1	0.99	2.85	3.3970(14)	115	
C9-H9...O3	0.95	2.31	3.1211(15)	143	$-1/2 + x, 3/3 + y, z$

Table 2. Cont.

D-H...A	d(D-H)	d(H...A)	d(D...A)	<(DHA)	Symmetry Code
<b>4</b>					
N1-H1...O2	0.92(3)	1.77(3)	2.682(2)	174(2)	$x, -1 + y, z$
N3-H3A...O1	0.92(3)	1.90(3)	2.814(2)	173(2)	$x, -1 + y, z$
N3-H3B...N2	0.89(3)	2.19(3)	3.080(3)	174(3)	$-x, -y, -z$
O4-H4...O2	0.98(3)	1.54(3)	2.518(2)	175(3)	$-1 + x, -1 + y, z$
N4-H4A...O5	0.87(3)	2.08(3)	2.854(3)	149(2)	$-x, 1 - y, -z$
N4-H4B...O3	0.88(3)	2.17(3)	3.049(2)	177(3)	$1 - x, 1 - y, -z$
O5-H5A...O1	0.90(3)	1.81(3)	2.685(2)	164(3)	
O5-H5B...O3	0.78(3)	2.14(3)	2.921(2)	177(3)	
C2-H2B...O5	0.99	2.58	3.524(3)	158	$1 + x, y, z$
C12-H12...O3	0.95	2.54	3.437(3)	157	$1 + x, y, z$

### 3.2. Supramolecular Features of 1–4

The crystal packing of all the analysed structures is shown in Figure 6 revealing various supramolecular architectures. In the crystals, the molecules are linked by numerous O-H...O, N-H...O, N-H...N, C-H...O contacts and in **3** additionally by C-H...S interactions (Table 2), enclosing diverse dimers (*D*) and ring motifs (*R*) at the first level of graph set theory [30] and *D*, *R* and *C* (chain) at the second level of graph set theory according to Etter's rules [30,31] (Table S3). As a consequence, these interactions link the molecules into 3D networks. It is worth mentioning that in **1**, a disorder of the water protons does not change significantly the H-bonding pattern (Tables 2 and S3). In this context, one additional motif is observed:  $D^2_3(5)$  via  $(\text{H}_2\text{O})\text{O5-H5C}\cdots\text{O5}_{(\text{H}_2\text{O})}$  and  $(\text{NH}_2)\text{N3-H3B}\cdots\text{O5}_{(\text{H}_2\text{O})}$  interactions.

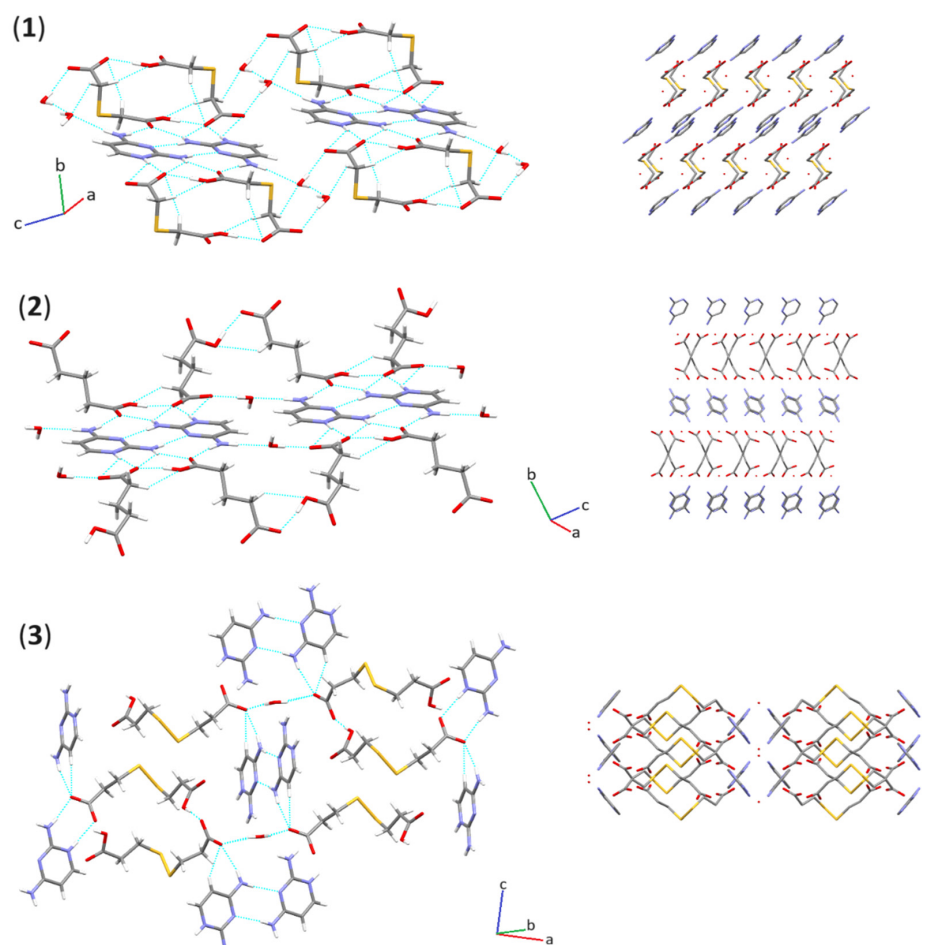
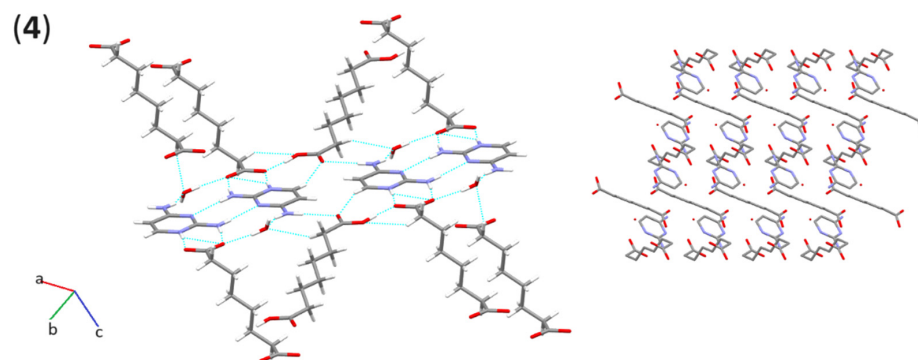
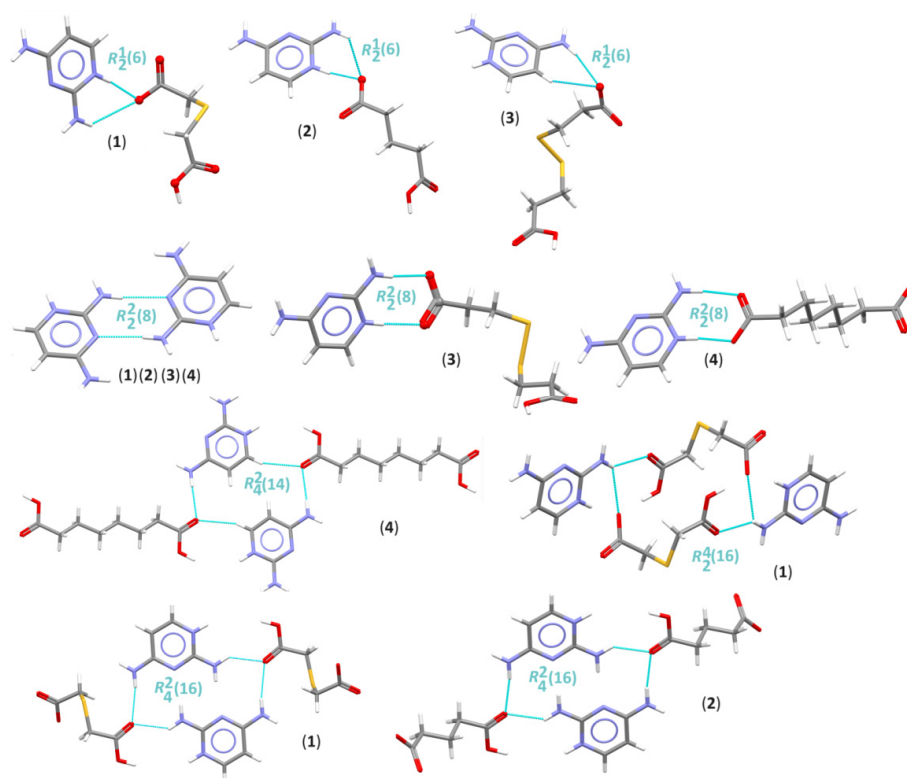


Figure 6. Cont.



**Figure 6.** Crystal packing diagrams of 1–4 compounds. For clarity, only one position of the disordered moiety is included.

Notably, 2,4-diaminopyrimidine is an appealing planar supramolecular tecton participating in the formation of diverse synthons. Figure 7 illustrates selected cyclic synthons observed in analysed crystals in all of the structures; the N-H $\cdots$ N interactions between 2,4-diaminopyrimidine molecules are the main association mode leading to  $R^2_2(8)$  homosynthon. In **1**, **2** and **3**, the carbonyl oxygen atom of anions plays the role of bifurcated acceptor in two N-H $\cdots$ O interactions, generating an  $R^1_2(6)$  motif. In all structures, a robust and the most popular synthon in organic compounds  $R^2_2(8)$  is observed: here either as homosynthon via N-H $\cdots$ N interactions in **1–4** or heterosynthon via N-H $\cdots$ O interactions in **3** and **4**. Furthermore, the same types of intermolecular contacts form larger cyclic heterosynthons— $R^4_2(16)$  in **1**,  $R^2_4(16)$  in **1** and **2**, and  $R^2_4(14)$  in **4**. It can be mentioned that the structure of the intermolecular interaction nets of analysed salts is also guided by the presence of stacking interactions as well. However, there are rather non-obvious  $\pi\cdots\pi$  interactions [32] only in **3** and **4**; shorter centroid-to-centroid distances between 2,4-diaminopyrimidine rings are observed (Table S1). Besides, the supramolecular structures of **1**, **3** and **4** are controlled by C-O $\cdots\pi$  intermolecular contacts (Table S2).



**Figure 7.** Selected cyclic synthons containing 2,4-diaminopyrimidine moiety observed in analysed salts.



Hirshfeld surface analysis was carried out using CrystalExplorer [33,34] to obtain more information on intermolecular interactions and their contribution to the supramolecular self-assemblies of 1–4 [26]. In all crystal structures, the types of intermolecular contacts are not only H···H, O···H/H···O, N···H/H···N, C···H/H···C, but also O···N/N···O, O···C/C···O, N···N and C···C. In addition, in 1 and 3, S···H/H···S interactions are observed, while in 1 S···C/C···S and S···N/N···S contacts are also observed (Figure 8, Table S4). H···H interactions are the most significant, contributing from 30% in 1 to 41% in 3 to the total crystal packing, due to van der Waals interactions [35].

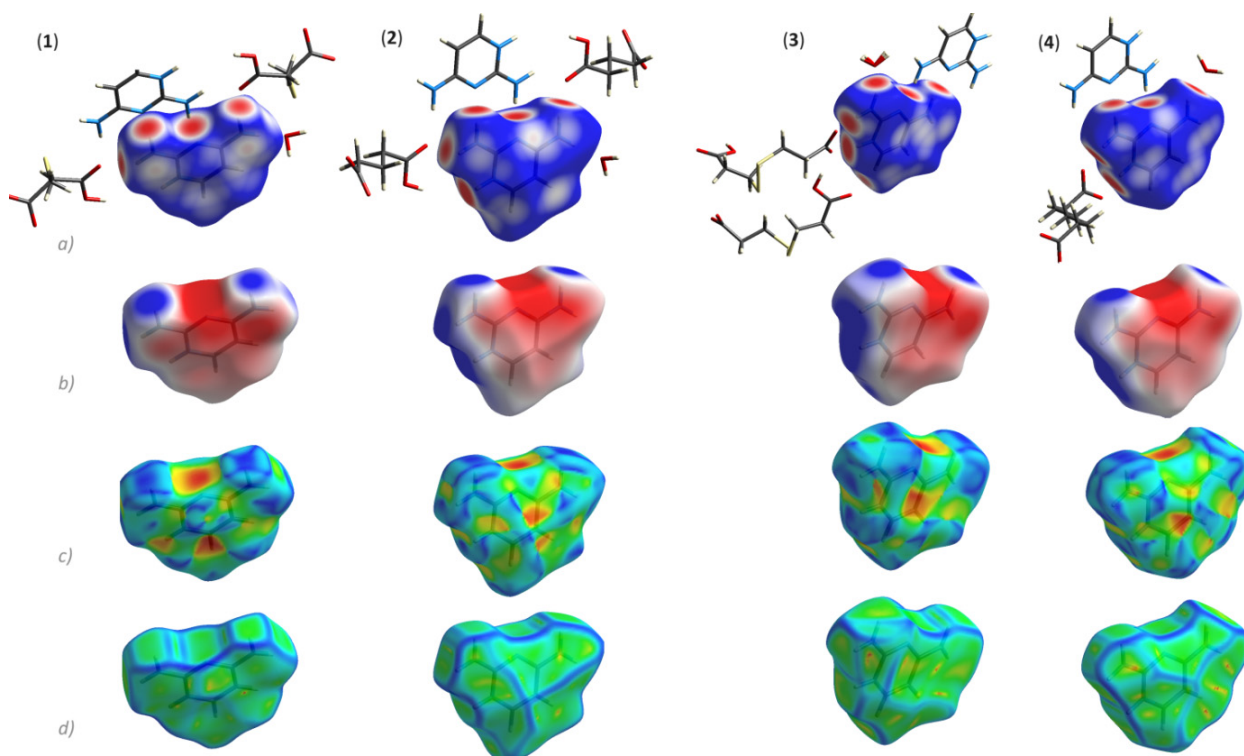


**Figure 8.** The Hirshfeld surface of 1–4 compounds mapped over: (a)  $d_{norm}$  showing the relevant close interactions, (c) *shape index* and (d) *curvedness*. In addition, molecular electrostatic potential mapped on Hirshfeld surface is presented (b).

3D maps for the 2,4-diaminopyrimidine moiety of 1–4 are shown in Figure 9. The shortest hydrogen bonds O···H/H···O and N···H/H···N contacts are represented via several red dots on the  $d_{norm}$ -maps, indicating these contacts as another one of the largest contributors to the Hirshfeld surfaces of 1–4, at the level of ~40% (Figures 8 and 9, Table S4). In addition, C···H/H···C contacts (~13%) and C···O/O···C contacts (~2%), are visualized on the *shape index* and *curvedness* maps. The red/blue triangles in the *shape index* and flat green areas in the *curvedness* signify  $\pi$ ··· $\pi$  stacking contacts, especially in 4 (Figure 9). The percentage share of O···H/H···O, N···H/H···N and C···H/H···C does not change drastically among the compounds. Although compounds 1 and 3 contain S-atoms, the percentage of S-based interactions is rather low. For example, in 1, the contribution of the S···H/H···S is 3.1%, while for 3 this contribution accounts for only 0.6% of all the contacts.

The 2D full fingerprint plots illustrating the distribution of all interactions in 1–4 are presented in Figure 9. A more diffused shape of the fingerprint of 2 may indicate lower packing efficiency than in the 1 counterpart [36], see the calculated Kitaigorodskii packing indexes (K.P.I.) of 69.9% for the former in contrast to 74.7% for the latter (Table 1) [25]. The enrichment ratios [29] were calculated to indicate the propensity for the setting up of specific intermolecular contacts in 1–4. The results revealed that S···C/C···S, S···N/N···S, O···H/H···O, N···C/C···N, C···H/H···C, N···H/H···N and

$N\cdots N$  of **1**,  $N\cdots C/C\cdots N$ ,  $O\cdots H/H\cdots O$ ,  $N\cdots H/H\cdots N$ ,  $C\cdots H/H\cdots C$  of **2**,  $N\cdots C/C\cdots N$ ,  $O\cdots H/H\cdots O$ ,  $O\cdots C/C\cdots O$ ,  $N\cdots H/H\cdots N$  and  $H\cdots H$  of **3** as well as  $O\cdots H/H\cdots O$ ,  $C\cdots C$ ,  $N\cdots H/H\cdots N$ ,  $C\cdots H/H\cdots C$ ,  $N\cdots C/C\cdots N$  of **4** have a ratio equal to or greater than unity, indicating these interactions play a key role in crystal packing. Notably,  $O\cdots H/H\cdots O$ ,  $N\cdots H/H\cdots N$ , and  $N\cdots C/C\cdots N$  interactions are favoured in all crystals, while  $C\cdots C$  is only in **4**,  $O\cdots C/C\cdots O$  is only in **3**, and  $S\cdots N/N\cdots S$ ,  $S\cdots C/C\cdots S$  and  $N\cdots N$  is only in **1**.

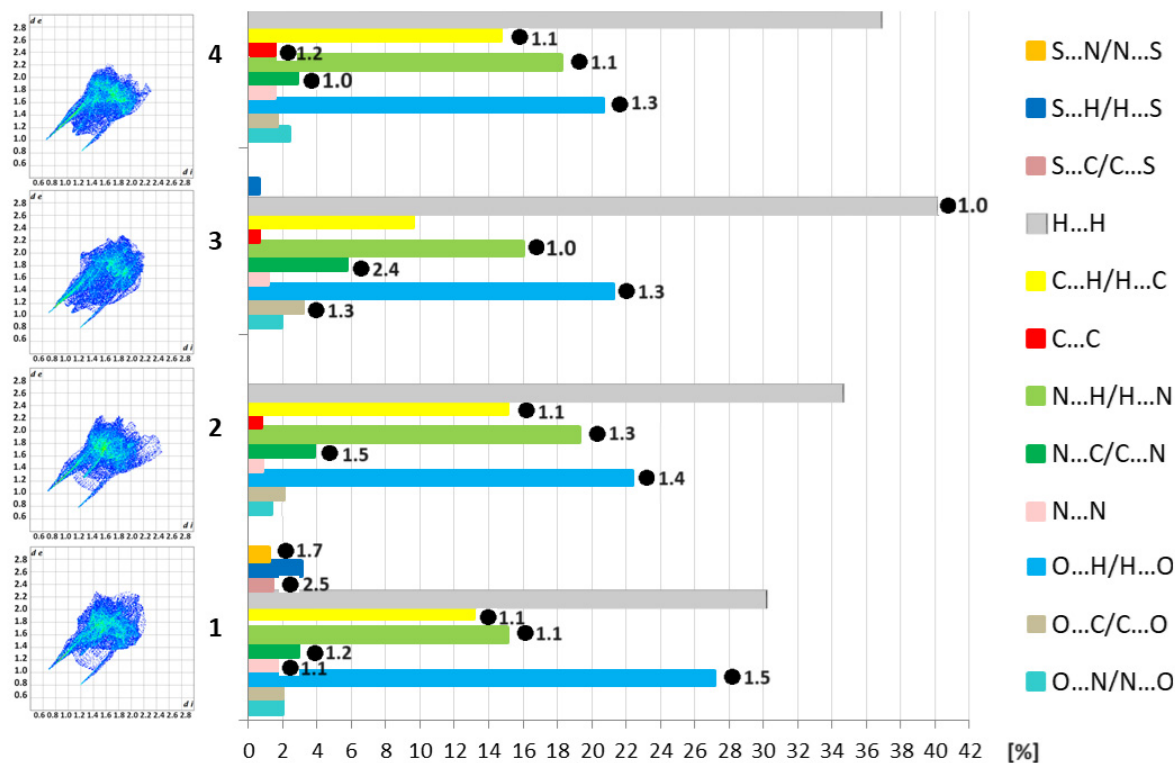


**Figure 9.** On the left: two-dimensional full fingerprint plots from Hirshfeld surfaces of 2,4-diaminopyrimidine moiety for **1–4**. On the right: the relative contributions of different types of intermolecular interactions in crystals **1–4** on the basis of Hirshfeld surface analysis. The calculated enrichment ratios greater than unity (including percentage distribution) are signified by black dots.

#### 4. Conclusions

The synthesis of 2,4-diaminopyrimidine salts by a straightforward reaction of 2,4-diaminopyrimidine and selected dicarboxylic acids in water was accomplished. Despite the similarity in molecular structures of **1** and **2** as well as **3** and **4**, their molecular packing show quite distinct supramolecular features. This is illustrated by the different molecular arrangements leading to diverse supramolecular heterosynthons formed at the upper level of supramolecular architecture of the considered crystals, especially cyclic motifs such as  $R^4_2(16)$  in **1**, and  $R^2_4(16)$  in **2** via  $(NH_2)N-H\cdots O(COO^-)$  interactions as well as  $R^2_4(14)$  via  $(cyc)C-H\cdots O(COOH)$  in **4**, that is not observed in **3**. Notably, a prominent homosynthon  $R^2_2(8)$  generated via  $N-H\cdots N$  interactions is observed in the crystal lattice of all structures, albeit with the participation of different anions. The presence of water molecules in the unit cell offers a greater possibility of generation of rich H-bonding supramolecular synthon patterns. Hirshfeld surface study and calculated enrichment ratios revealed that  $O\cdots H/H\cdots O$ ,  $N\cdots H/H\cdots N$ ,  $C\cdots H/H\cdots C$ ,  $N\cdots C/C\cdots N$ , but also  $S\cdots C/C\cdots S$ ,  $S\cdots N/N\cdots S$  and  $N\cdots N$  in **1**,  $O\cdots C/C\cdots O$  in **3**, while  $C\cdots C$  interactions in **4** are key in stabilization of the supramolecular self-assemblies of **1–4**.

**Supplementary Materials:** The following supporting information can be downloaded at: <https://www.mdpi.com/article/10.3390/cryst14020133/s1>. Table S1. Geometric parameters of  $\pi \cdots \pi$  interactions observed in the crystals 1–4 (only distances  $Cg \cdots Cg < 5 \text{ \AA}$  are shown); Table S2. Geometric parameters of  $C-O \cdots \pi$  interactions observed in the crystals 1–4; Table S3. Percentage contributions of close intercontacts in the crystals 1–4 (Hirshfeld surface analysis for 2,4-diaminopyrimidine motif); Table S4. Gallery of H-bonding supramolecular synthons containing 2,4-diaminopyrimidine moiety.

**Author Contributions:** Conceptualization, A.M.; methodology, A.M. and K.L.; validation, K. L. and J.B.; formal analysis, K.L. and J.B.; investigation, K.L., J.B. and A.M.; data curation, K.L. and J.B.; writing—original draft preparation, K.L., J.B. and A.M. All authors have read and agreed to the published version of the manuscript.

**Funding:** This research received no external funding.

**Data Availability Statement:** CCDC 2320888-2320891 contain the supplementary crystallographic data for this paper, accessed on 20 December 2023. These data can be obtained free of charge via <https://www.ccdc.cam.ac.uk/structures>.

**Conflicts of Interest:** The authors declare no conflicts of interest.

## References

1. Ashique, S.; Sandhu, N.K.; Haque, S.N.; Koley, K. A Systemic Review on Topical Marketed Formulations, Natural Products, and Oral Supplements to Prevent Androgenic Alopecia: A Review. *Nat. Prod. Bioprospect.* **2020**, *10*, 345–365. [CrossRef]
2. Wróbel, A.; Ariszewska, K.; Maliszewski, D.; Drozdowska, D. Trimethoprim and other nonclassical antifolates an excellent template for searching modifications of dihydrofolate reductase enzyme inhibitors. *J. Antibiot.* **2020**, *73*, 5–27. [CrossRef]
3. Raimondi, M.V.; Randazzo, O.; La Franca, M.; Barone, G.; Vignoni, E.; Rossi, D.; Collina, S. DHFR Inhibitors: Reading the Past for Discovering Novel Anticancer Agents. *Molecules* **2019**, *24*, 1140. [CrossRef]
4. Ai, M.; Wang, C.; Tang, Z.; Liu, K.; Sun, X.; Ma, T.; Li, Y.; Ma, X.; Chen, L. Design and synthesis of diphenylpyrimidine derivatives (DPPYs) as potential dual EGFR T790M and FAK inhibitors against a diverse range of cancer cell lines. *Bioorg. Chem.* **2020**, *94*, 103408. [CrossRef]
5. Wang, S.; Zhang, R.-G.; Zhang, H.; Wang, Y.-C.; Yang, D.; Zhao, Y.-L.; Yan, G.-Y.; Xu, G.-B.; Guan, H.-Y.; Zhou, Y.-H.; et al. Design, synthesis, and biological evaluation of 2,4-diamino pyrimidine derivatives as potent FAK inhibitors with anti-cancer and anti-angiogenesis activities. *Eur. J. Med. Chem.* **2021**, *222*, 113573. [CrossRef]
6. Matulkova, I.; Mathauserova, J.; Cisarova, I.; Nemeč, I.; Fabry, J. The study of crystal structures and vibrational spectra of inorganic salts of 2,4-diaminopyrimidine. *J. Mol. Struct.* **2016**, *1103*, 82–93. [CrossRef]
7. Bertolasi, V.; Pretto, L.; Gilli, P.; Ferretti, V.; Gilli, G. Hydrogen-bonded supramolecular structures in co-crystals of  $\beta$ - or  $\zeta$ -diketone enols with 2,6-diaminopyridine or 2,4-diaminopyrimidine. *New J. Chem.* **2002**, *26*, 1559–1566. [CrossRef]
8. Draguta, S.; Fonari, M.S.; Masunov, A.E.; Zazueta, J.; Sullivan, S.; Antipin, M.Y.; Timofeeva, T.V. New acentric materials constructed from aminopyridines and 4-nitrophenol. *CrystEngComm* **2013**, *15*, 4700–4710. [CrossRef]
9. Hutzler, W.M.; Egert, E.; Bolte, M. One barbiturate and two solvated thiobarbiturates containing the triply hydrogen-bonded ADA/DAD synthon, plus one ansovate and three solvates of their cofomer 2,4-diaminopyrimidine. *Acta Cryst. C* **2016**, *72*, 705–715. [CrossRef]
10. Hutzler, W.M.; Egert, E.; Bolte, M. 6-Propyl-2-thiouracil versus 6-methoxymethyl-2-thiouracil: Enhancing the hydrogen-bonded synthon motif by replacement of a methylene group with an O atom. *Acta Cryst. C* **2016**, *72*, 634–646. [CrossRef]
11. Hall, V.M.; Thornton, A.; Miehl, E.K.; Bertke, J.A.; Swift, J.A. Uric Acid Crystallization Interrupted with Competing Binding Agents. *Cryst. Growth Des.* **2019**, *19*, 7363–7371. [CrossRef]
12. Bis, J.A.; Zaworotko, M.J. The 2-Aminopyridinium-carboxylate Supramolecular Heterosynthon: A Robust Motif for Generation of Multiple-Component Crystals. *Cryst. Growth Des.* **2005**, *5*, 1169–1179. [CrossRef]
13. Mirzaei, M.; Sadeghi, F.; Molčanov, K.; Zareba, J.K.; Gomila, R.M.; Frontera, A. Recurrent Supramolecular Motifs in a Series of Acid–Base Adducts Based on Pyridine-2,5-Dicarboxylic Acid N-Oxide and Organic Bases: Inter- and Intramolecular Hydrogen Bonding. *Cryst. Growth Des.* **2020**, *20*, 1738–1751. [CrossRef]
14. Ebenezer, S.; Muthiah, P.T. Design of Co-crystals/Salts of Aminopyrimidines and Carboxylic Acids through Recurrently Occurring Synthons. *Cryst. Growth Des.* **2012**, *12*, 3766–3785. [CrossRef]
15. Capelletti da Silva, C.; de Lima Cirqueira, M.; Martins, F.T. Lamivudine salts with 1,2-dicarboxylic acids: A new and a rare synthon with double pairing motif fine-tuning their solubility. *CrystEngComm* **2013**, *15*, 6311–6317. [CrossRef]
16. Garg, U.; Azim, Y.; Kar, A.; Pradeep, C.P. Cocrystals/salt of 1-naphthaleneacetic acid and utilizing Hirshfeld surface calculations for acid–aminopyrimidine synthons. *CrystEngComm* **2020**, *22*, 2978–2989. [CrossRef]
17. Janczak, J. Structure, vibrational characterization and DFT calculations of 1-(diaminomethylene)thiourea-1-ium 2,3-pyridinedicarboxylate. *Struct. Chem.* **2023**. [CrossRef]

18. Clarke, H.D.; Arora, K.K.; Bass, H.; Kavuru, P.; Ong, T.T.; Pujari, T.; Wojtas, L.; Zawarotko, M.J. Structure–Stability Relationships in Cocrystal Hydrates: Does the Promiscuity of Water Make Crystalline Hydrates the Nemesis of Crystal Engineering? *Cryst. Growth Des.* **2019**, *10*, 2152–2167. [[CrossRef](#)]
19. Surov, A.O.; Vasilev, N.A.; Churakov, A.V.; Parashchuk, O.D.; Artobolevskii, S.V.; Alatorsev, O.A.; Makhrov, D.E.; Vener, M.V. Two Faces of Water in the Formation and Stabilization of Multicomponent Crystals of Zwitterionic Drug-Like Compounds. *Symmetry* **2021**, *13*, 425. [[CrossRef](#)]
20. Bolla, G.; Nangia, A. Novel pharmaceutical salts of albendazole. *CrystEngComm* **2018**, *20*, 6394–6405. [[CrossRef](#)]
21. Hu, L.; Staples, R.J.; Shreeve, J.M. Energetic compounds based on a new fused triazolo[4,5-d]pyridazine ring: Nitroimino lights up energetic performance. *Chem. Eng. J.* **2021**, *420*, 129839. [[CrossRef](#)]
22. Sheldrick, G.M. Crystal Structure Refinement with SHELXL. *Acta Cryst. C* **2015**, *71*, 3–8. [[CrossRef](#)]
23. Dolomanov, O.V.; Bourhis, L.J.; Gildea, R.J.; Howard, J.A.K.; Puschmann, H. OLEX2: A complete structure solution, refinement and analysis program. *J. Appl. Crystallogr.* **2009**, *42*, 339–341. [[CrossRef](#)]
24. Macrae, C.F.; Sovago, I.; Cottrell, S.J.; Galek, P.T.A.; McCabe, P.; Pidcock, E.; Platings, M.; Shields, G.P.; Stevens, J.S.; Towler, M.; et al. Mercury 4.0: From visualization to analysis, design and prediction. *J. Appl. Cryst.* **2020**, *53*, 226–235. [[CrossRef](#)]
25. Spek, A.L. Structure Validation in chemical crystallography. *Acta Cryst. D* **2009**, *65*, 148–155. [[CrossRef](#)]
26. Turner, M.J.; McKinnon, J.J.; Wol, S.K.; Grimwood, D.J.; Spackman, P.R.; Jayatilaka, D.; Spackman, M.A. *CrystalExplorer*, version 3.1; The University of Western Australia: Perth, Australia, 2017.
27. Spackman, M.A.; Jayatilaka, D. Hirshfeld surface analysis. *CrystEngComm* **2009**, *11*, 19–32. [[CrossRef](#)]
28. Jayatilaka, D.; Grimwood, D.J. Tonto: A Fortran Based Object-Oriented System for Quantum Chemistry and Crystallography. In *Computational Science—ICCS 2003*; Sloot, P.M.A., Abramson, D., Bogdanov, A.V., Gorbachev, Y.E., Dongarra, J.J., Zomaya, A.Y., Eds.; Lecture Notes in Computer Science; Springer: Berlin/Heidelberg, Germany, 2003; Volume 2660, pp. 142–151. [[CrossRef](#)]
29. Jelsch, C.; Ejsmont, K.; Huder, L. The enrichment ratio of atomic contacts in crystals, an indicator derived from the Hirshfeld surface analysis. *IUCrJ* **2014**, *1*, 119–128. [[CrossRef](#)]
30. Bernstein, J.; Davis, R.E.; Shimoni, L.; Chang, N.L. Patterns in Hydrogen Bonding: Functionality and Graph Set Analysis in Crystals. *Angew. Chem. Int. Ed.* **1995**, *34*, 1555–1573. [[CrossRef](#)]
31. Etter, M.C. Encoding and decoding hydrogen-bond patterns of organic compounds. *Acc. Chem. Res.* **1990**, *23*, 120–126. [[CrossRef](#)]
32. Nishio, M. CH/interactions hydrogen bonds in crystals. *CrystEngComm* **2004**, *6*, 130–158. [[CrossRef](#)]
33. Spackman, P.R.; Turner, M.J.; McKinnon, J.J.; Wolff, S.K.; Grimwood, D.J.; Jayatilaka, D.; Spackman, M.A. *CrystalExplorer*: A program for Hirshfeld surface analysis, visualization and quantitative analysis of molecular crystals. *J. Appl. Cryst.* **2021**, *54*, 1006–1011. [[CrossRef](#)] [[PubMed](#)]
34. McKinnon, J.J.; Jayatilaka, D.; Spackman, M.A. Towards quantitative analysis of intermolecular interactions with Hirshfeld surfaces. *Chem. Commun.* **2007**, *37*, 3814–3816. [[CrossRef](#)] [[PubMed](#)]
35. Hathwar, V.R.; Sist, M.; Jørgensen, M.R.V.; Mamakhel, A.H.; Wang, X.; Hoffmann, C.M.; Sugimoto, K.; Overgaard, J.; Iversen, B.B. Quantitative analysis of intermolecular interactions in orthorhombic rubrene. *IUCrJ* **2015**, *2*, 563–574. [[CrossRef](#)]
36. Lee, S.M.; Lo, K.M.; Tan, S.L.; Tiekink, E.R.T. (Tris{2-[(5-chloro-2-oxido benzyl idene-κO)amino-κN]ethyl}amine-κN) ytterbium(III): Crystal structure and Hirshfeld surface analysis. *Acta Crystallogr. E* **2016**, *72*, 1390–1395. [[CrossRef](#)] [[PubMed](#)]

**Disclaimer/Publisher’s Note:** The statements, opinions and data contained in all publications are solely those of the individual author(s) and contributor(s) and not of MDPI and/or the editor(s). MDPI and/or the editor(s) disclaim responsibility for any injury to people or property resulting from any ideas, methods, instructions or products referred to in the content.